Fermi National Accelerator Laboratory

Fermilab-Pub/88-135-T
September 1988

SMALL-X BEHAVIOR OF PARTON DISTRIBUTION FUNCTIONS IN THE NEXT-TO-LEADING ORDER QCD PARTON MODEL

Wu-Ki Tung†

Illinois Institute of Technology, Chicago IL 60616

and

Fermi National Accelerator Laboratory, Batavia IL 60510

Abstract

The systematic application of QCD-based parton model to the quantitative analyis of high energy processes requires reliable parton distributions including 2nd-order QCD evolution effects — both for consistency and for accuracy, especially in exceptional kinematic regimes such as the small-x region. We discuss qualitative expectations and present quantitative results on the behavior of 2nd-order evolved parton distributions in this region which is particularly important for studying physical processes at future accelerators. Direct comparisons with recently available 2nd-order parton distributions are made in order to check consistency for future studies of high energy processes. Also presented are quantitative results on the scheme-dependence of parton distributions in the next-to-leading order approximation.

† This work is supported in part by the National Science Foundation Grant No. PHY-85-07635.

A. RELEVANCE OF SECOND-ORDER QCD EVOLUTION OF PARTON DISTRIBUTIONS

The QCD-based Parton Model provides the framework for most contemporary studies of high-energy physical processes at current and future accelerators. Comparisons of a wide variety of physical cross-sections calculated in this scheme to *Leading Order* in the QCD effective coupling with experiment have led to remarkable qualitative confirmation of the underlying theoretical framework and furnished the basis for a unified approach to all high energy processes. In particular, the ability to use the renormalization group technique to calculate the *evolution* of universal *parton distribution functions* to large energy scales beyond those currently available provides a powerful tool to extend standard model predictions to future accelerator ranges and to prepare for new discoveries. Recent studies have called attention to the limitations of leading order calculations in exceptional kinematic regions and for special processes. To achieve quantitative understanding of the QCD-based parton model and to use it with confidence in projecting physical results at future energies, it has become necessary to include additional terms beyond the leading order in a systematic and self-consistent manner.

To make our discussions more concrete, let us write the basic formula for a generic high-energy process

$$A + B \longrightarrow C + X \qquad (1)$$

in the QCD-based parton model as

$$\sigma_{AB\to CX} = f_A^a \otimes \hat{\sigma}_{ab\to C} \otimes f_B^b \qquad (2)$$

where $f_A{}^a$ is the distribution function of parton a in the hadron A, $\hat{\sigma}$ is the *hard scattering* cross-section for the partonic process, and $\otimes$ denotes a convolution integral in the fractional momentum variable for the parton involved. The **leading order approximation** involves keeping only the lowest non-vanishing term in the perturbation series expansion of the hard cross-section $\hat{\sigma}$ and of using scale-dependent parton distributions $f_A{}^a$ obtained by solving the *QCD evolution equations* with 1-loop splitting functions.

In recent years attention has increasingly been drawn to the importance of *Next to Leading Order* corrections to the hard cross-section $\hat{\sigma}$ for the Drell-Yan process,[1] to direct photon production,[2] to inclusive 2 jet-production,[3] and to heavy flavor production.[4] In order to explore the full physical implication of these results it is important also to understand the behavior of parton distribution functions calculated to the corresponding order in the QCD perturbation expansion. In fact, this is absolutely *required* because both $\hat{\sigma}$ and $f_A{}^a$, as they appear on the right-hand side of Eq.(2), are *renormalization-scheme-dependent* (as well as scale-dependent) beyond the leading order approximation. Since the physical cross-section on the left-hand side cannot depend on the renormalization scheme, one must use hard cross-sections and parton distribution functions defined in the same scheme and calculated to a consistent order to obtain meaningful results. Specifically, *the study of 1-loop corrections to the hard cross-section requires the use of the matching distribution functions obtained with 2-loop evolution kernels.* Together, they provide the **Next-to-Leading-Approximation** to the physical cross-section in the QCD-based parton model formalism.

Nominally, the inclusion of the second-order evolution kernel in the calculation of the scale-dependent parton distribution functions yields order α_s/π corrections to the leading order results. However, this is not necessarily true over all kinematic regions. Just as for the case of hard scattering cross-section,[1-4] there are circumstances under which the higher order kernel can be significant, or even dominant, compared to the leading one. This consideration is especially relevant at present since the study of high energy processes at current and future colliders places more and more emphasis on the "small-x" region, where the parton momentum fraction variable x is approximately the ratio of the physical energy scale of interest to the total available energy of the collision. An essential feature of all such studies is that predicted cross-sections depend critically on the rapid growth of the parton distribution functions with the energy scale in the small-x region. In many respects, *the small-x region beyond currently measurable (about x = 0.01) is an exceptional kinematic region.*[5] It is therefore extremely important to determine how the evolution of the parton distribution functions with the energy scale in this region is affected by the inclusion of higher order QCD effects.

Several parton distribution function calculations including 2-loop evolution effects have been performed in the context of QCD analysis of existing deep inelastic scattering (and other lepton-hadron scattering) data.[6,7,8,9,10] For reasons described above, this paper focuses more on the implications of the second order kernel for the predicted behavior of parton distributions in the small-x region beyond the currently accessable range (sections B & C). In view of the increasing importance of the second-order distributions and the complexity of the calculations involved, we also engage in the first systematic comparison of available new parton distribution sets to assess the reliability of these "second generation" distributions (section D). As we shall see, the result of this comparison is mixed. Finally, we present quantitative results on the non-trivial **scheme dependence** of the parton distributions beyond the leading order (section E).

B. CALCULATION OF PARTON DISTRIBUTIONS INCLUDING 2-LOOP EVOLUTION KERNELS

The renormalization equation for the parton distribution functions reads:

$$Q \frac{d}{2dQ} f_A^a(x,Q) = P(x,\alpha_\pi)_b^a \otimes f_A^b(x,Q) \qquad (3)$$

with $\alpha_\pi \equiv \alpha_s(Q)/2\pi$ and

$$P(x,\alpha_\pi) = \alpha_\pi [\, P_1(x) + \alpha_\pi \cdot P_2(x) + \cdots \,] \qquad (4)$$

The first order kernel $P_1(x)$ is well-known. The complete second-order kernel $P_2(x)$ is quite involved;[11] there is no need to reproduce it here. For reasons mentioned in the introduction, however, it is useful to focus on the small-x region where the latter may have a significant impact.

The evolution kernel can be partially diagonalized. To second-order, it consists of two uncoupled *non-singlet* pieces $P_{NS}(x)^{\pm}$ and a 2x2 *singlet* matrix which couples the gluon and the singlet quark distributions.[12] The non-singlet kernels do not contain terms

more singular than $(ln\ x)$ at small x. The most singular terms of the singlet kernel functions at small x are proportional to $1/x$. (A cursory look at the expressions for $P_2(x)$ may indicate the presence of ln^2x/x as well as $(ln\ x)/x$ terms. However, in the MS-bar scheme these terms cancel in the end.[13]) Table 1 displays the leading terms of these second-order kernel functions in the small-x region along with the familiar first-order kernel functions.

	1-Loop	2-Loop
$P(x)^F{}_F$	$C_F \frac{1+x^2}{1-x} + \ldots$	$2N_f T_R C_F \frac{20.}{9} \frac{1}{x} + \cdots$
$P(x)^F{}_G$	$2N_f T_R [x^2 + (1-x^2)]$	$2N_f T_R C_G \frac{20.}{9} \frac{1}{x} + \cdots$
$P(x)^G{}_F$	$C_F \frac{1}{x} [1 + (1-x)^2]$	$2N_f T_R C_F (-\frac{20.}{9} \frac{1}{x}) + C_F C_G \frac{1}{x} + \cdots$
$P(x)^G{}_G$	$2C_G [\frac{1}{x} + \frac{1}{1-x} - 2 + x - x^2] + \ldots$	$\frac{2N_F T_R}{x} [-\frac{23.}{9} C_G + \frac{2}{3} C_F] + \cdots$

Table 1: Comparison of 1-Loop & 2-Loop Kernels at Small-x

Two features of the results in this Table are worth noting. First, *the second-order kernel functions $P_2(x)^F{}_F$ and $P_2(x)^F{}_G$ contain the singular $1/x$ terms whereas the corresponding first-order kernel functions $P_1(x)^F{}_F$ and $P_1(x)^F{}_G$ don't.* This singular part, of course, easily overwhelms the α_π factor multiplying the second-order kernel. Hence, the evolution of the fermion (quarks and anti-quarks) distribution functions at small-x will be completely dominated by the second-order kernel rather than the first-order one. Second, *the $1/x$ terms in $P_2(x)^G{}_G$ and $P_2(x)^G{}_F$ are large in magnitude and opposite in sign with respect to the corresponding terms in the first order kernel functions.* Thus, the well-known rapid growth of the gluon distribution at small-x seen in the usual leading order calculations will be dampened by the inclusion of next-to-leading terms. These features confirms the importance of studying the effects of the second-order kernel in quantitative detail.

We solve numerically the integral-differential evolution equation, Eq.(3), with arbitrary input distribution functions at a fixed value of Q ("Q_0") and arbitrary QCD parameters Λ_{QCD}, N_f (# of quark flavors) and quark masses. A previously available first-order evolution program[14] was rewritten to incorporate the much more complex second-order kernel with particular attention to maintaining the efficiency of the numerical calculation. In addition to performing the standard sum-rule tests, the new program, which uses a new algorithm, was checked against the original one for accuracy. (The latter has been extensively checked against other existing first-order parton distribution calculations in the literature.) Intermediate results in the calculation were systematically plotted and

compared to expected qualitative behavior, in magnitudes and signs, of the analytic expressions for the kernels and found to be satisfactory. The results presented below are based on these calculations.

C. SMALL-X BEHAVIOR OF PARTON DISTRIBUTION FUNCTION INCORPORATING 2ND-ORDER EFFECTS

In order to see the effects due to the second-order evolution kernel, we first compare parton distribution functions calculated with and without the $P_2(x)$ term in Eq.(4) using the same effective coupling α_s and the same input distribution functions at Q_0. Fig.1 shows some typical results obtained with the EHLQ distribution[15] Set 1 as input at Q_0 = 4.0 GeV.

Plotted in Fig.1a are the u-quark distribution in the range $10^{-4} < x < 0.8$ at the scale Q = 15 GeV obtained with 1st-order (dotted line) and 1st-plus-2nd-order (solid line) evolution kernels. We see that the latter shows a much stronger growth at small x. This is clear evidence of effects due to the positive 1/x terms in the 2nd order kernel functions $P_2(x)^F{}_F$ and $P_2(x)^F{}_G$ (absent in the leading order) as described in the previous section. The difference of the two distributions at $x = 10^{-4}$ is about 30%; this shrinks to a few percent above x = 0.01.

In Fig.1b we show the corresponding results on the gluon distribution. In contrast to the fermion case, the 2nd order calculation yields a flatter gluon distribution than the the leading order one. This is, again, expected from the discussion of the previous section — the most singular terms at small x for the 2nd order kernel have large coefficients (to partially compensate for the extra coupling factor) and are opposite in sign to those of the leading order ones.

Figs.1c & 1d show the corresponding plots of the u-quark and the gluon distributions at Q = 100 GeV. The features are similar to those described for the 15 GeV case. Table 2 quantifies the results shown in these plots. The distribution functions for other quark flavors, not shown explicitly here, have analogous behavior. In particular, the anti-u and anti-d quark distributions almost coincide with the corresponding quark distributions at small x (due to the vanishing of the valence distributions at small x).

D. COMPARISON WITH OTHER 2ND-ORDER CALCULATIONS

Because of the significance of the 2nd order evolution in the small-x region where rapid growth of the distributions takes place, it is of interest to compare different 2nd order calculations of the QCD-evolved parton distribution functions in order to gain confidence in the predictions at high energies. These results are also becoming more and more important for quantitative next-to-leading-order QCD parton model analyses of current collider experiments.[1-4] The currently available distributions cannot be calibrated against each other because they are obtained from different initial distributions by fitting different sets of experimental data. We decided to perform direct comparisons of recently published parton distribution sets with corresponding ones generated by our calculation using identical input distributions and (essentially) the same QCD parameters.

We obtain good agreement with the next-to-leading-order distribution functions of DFLM[8] (the set labelled FXNLLA available from the authors). In order to obtain a meaningful comparison in this case, we should note that this set of distributions is defined in a special renormalization scheme in which the deep inelastic scattering structure function F_2 retains its simple relation to the parton distribution functions as in the naive parton model. (We should refer to this as the **DIS scheme**; cf. Section E.) Thus, for the comparison, we take the DFLM distributions at Q = 4 GeV, transform them into MS-bar scheme distributions, then use the latter as input distributions to our evolution calculation (which is based on the standard MS-bar scheme formulas for the kernels). The outcome of this calculation is then compared with the DFLM distributions at arbitrary Q, again, transformed into the MS-bar scheme at the relevant scale Q. Representative results of this comparison are given in Table 3. The agreement is in general within a few percent. This is acceptable considering the fact that interpolation formulas are used in extracting these numbers from the respective sets, that the DIS-to-MS-bar transformation induces errors at some level, and that minor differences in the definition of the coupling α_s and in the treatment of heavy quark thresholds may exist. It is worth noting that the DFLM calculation is carried out in the *moment space* which involves the solution of a set of coupled ordinary differential equations and the subsequent application of a delicate inverse Mellin transform; whereas our calculation is done in *x-space* which involves the solution of a set of coupled integral-differential equations. It is reassuring to see that the two entirely distinct methods yield consistent results.

A similar comparative study is carried out on the recently available MRS distributions.[7] Here we did not obtain acceptable agreement. This comparison is in principle simpler than the above, because the MRS distributions are defined in the *MS-bar scheme*. We can therefore use their distributions at a given Q_0, unmodified, as input; perform the evolution calculation; and compare directly the results at any Q. Fig.2 summarizes the main features of this comparison. The initial value Q_0 used for this calculation is 3 GeV.

In Fig.2a we show the u-quark distribution at Q = 15 GeV. Three curves are drawn: the MRS distribution as provided by the authors[7] (dotted line), the 2nd-order QCD-evolved distribution according to our calculation (solid line), and (for reference later) the 1st-order QCD-evolved distribution using the same coupling and input distributions (dashed line). The first two curves agree within 1% above $x = 10^{-2}$; however, they disagree in the small x region — differing by about 30% at $x = 10^{-4}$. The MRS distribution shows a much sharper rise in the small x region than our calculation. With respect to the 1st-order calculation, the MRS distribution is 60% larger at $x = 10^{-4}$ compared to 30% for our 2nd-order calculation. (Cf. also the results presented in Sec.C.)

Fig.2b shows the corresponding results for the gluon distribution. The difference here is even more dramatic. Whereas our 2nd-order curve lies *below* the 1st-order one (by several percent) at small x, the MRS distribution *rises much faster than* the latter — being larger by about 50% at $x = 10^{-4}$! This behavior seems to contradict the expectation based on inspection of the dominant terms of the evolution kernel at small-x as described in Sec.B. Above $x = 10^{-2}$, the two 2nd-order distributions approach each other, as seen in the figure; however, they do not agree as well as in the case of the u-quark — there is about a 5% discrepency.

Fig.2c and Fig.2d show the same distributions as those in Figs.2a & 2b at the higher energy scale Q = 100 GeV. The features are similar to those discussed above. The comparison of other quark- and anti-quark distributions (not shown here) reveal similar features as those for the u-quark.

E. THE DIS- vs. THE MS-SCHEME DISTRIBUTIONS

Second-order evolved parton distribution functions are necessarily renormalization-scheme dependent -- since the perturbatively calculated Wilson coefficients are renormalization-scheme dependent whereas the physically measurable structure functions are not. (Cf. Eq.(2)) In practical calculations it is useful to acquire knowledge about the actual size of the differences between the commonly used schemes for the various parton distributions in important kinematic regions. This section addresses this question.

There are two schemes of practical interest. The MS-bar subtraction scheme is a standard scheme to perform perturbative calculations of both hard cross-sections (Wilson coefficients) and evolution kernels (anomalous dimensions). We refer to parton distributions so defined as **MS-bar scheme** ones. It is process-independent and is applicable to all orders of perturbation expansion.

The other often used scheme, called the **DIS scheme** in Section D, is defined by the practical requirement that the most commonly encountered deep inelastic scattering structure function F_2 retain its leading-order relationship to the parton distribution functions even in the next-to-leading approximation. This amounts to absorbing the 1-loop MS-bar Wilson coefficients for F_2 into the definition of the parton distribution functions. The limitations of the DIS-scheme are: (i) it is only viable in the next-to-leading approximation (i.e. it cannot be generalized to higher orders); (ii) the other structure functions F_3 and F_L are not simple in terms of the parton distributions; and (iii) there is no natural definition of the gluon definition (beyond the obvious requirement of the momentum sum rule).

The quark distribution functions $f^a(x,Q)_D$ in the DIS scheme are defined in terms of the MS-bar scheme quark distributions $f^a(x,Q)_M$ and gluon distribution $f^G(x,Q)_M$ as:

$$f^a(x,Q)_D = (1 + \alpha_\pi C_q^2(x)) \otimes f^a(x,Q)_M + \alpha_\pi C_G^2(x) \otimes f^g(x,Q)_M \qquad (5)$$

where $C^2_{q,G}$ are the well-known Wilson coefficients.[16] Whereas there is no unique way of defining the gluon distribution in the DIS-scheme, for the purpose of the following comparison, we use the following definition:[8]

$$f^g(x,Q)_D = (1 + 2\alpha_\pi N_f C_G^2(x)) \otimes f^g(x,Q)_M + \alpha_\pi C_q^2(x) \otimes f^s(x,Q)_M \qquad (6)$$

where $f^s(x,Q)$ is the singlet quark distribution defined as the quark distribution summed over all flavors. (This prescription amounts to extending, arbitrarily, the momentum sum-rule relation to all moments of the distributions.)

Figure 3 shows typical results on the transformation between parton distributions in the two distinct schemes. As we can see, whereas these two sets of distributions are distinct at Q = 4 GeV, they become quite close to each other at Q = 15 GeV. This is expected, since α_s becomes small at large Q, and since the Wilson coefficients which enter Eqs.(5) and (6) are well behaved.

F. CONCLUSIONS

The systematic application of QCD-based parton model to the quantitative analyis of high energy processes requires reliable parton distributions including 2nd-order QCD evolution effects — both for consistency and for accuracy, especially in exceptional kinematic regimes such as the small-x region. We discussed qualitative expectations and presented quantitative results on the behavior of 2nd-order evolved parton distributions in this region which is particularly important for the study of physical processes at future accelerators. We also presented direct comparisons of our calculation with existing ones to help bring about consistent results for future studies of all high energy processes. Finally, since the definition of parton distribution functions necessarily becomes renormalization-scheme dependent, we presented concrete results on the transformation between the commonly used DIS- and MS-bar-schemes to display the quantitative features of this scheme-dependence for the quark- and gluon-distributions in typical kinematic regions.

ACKNOWLEDGEMENT

I have benefitted from many helpful discussions with John Collins, Keith Ellis, and Fred Olness. I also thank Dick Roberts and James Stirling for communications about their distributions.

REFERENCES

[1] G.Altarelli, R.K.Ellis, & G.Martinelli, Nucl. Phys. B143, 521 (1978), and *ibid.* B157, 461 (1979); J.Kubar-Andre & F. Paige, Phys. Rev. D19, 221 (1979).

[2] P. Aurenche *et. al.* Nucl. Phys. B297 661 (1988), and references cited therein.

[3] R.K. Ellis & J.Sexton, Nucl. Phys. B269, 445 (1986).

[4] P. Nason, S. Dawson and K. Ellis, Nucl. Phys. B303, 607 (1988).

[5] Proceedings of the 1984 Summer Study on the Design and Utilization of the SSC, Ed. R. Donaldson and J. Morfin, (1985); and Proceedings of the 1986 Summer Study on the Physics of the SSC, Ed. R. Donaldson and J. Marx, (1987).

[6] A.Devoto, D.Duke & J.Owens, Phys. Rev. D27, 508 (1983).

[7] A.D.Martin, R.G.Roberts & W.J.Stirling, Phys. Rev. D37, 1161 (1988).

[8] M.Diemoz, F.Ferroni, E.Longo & G.Martinelli, Z. Phys. C39, 21 (1988).

[9] H.Abramowicz *et. al.* (CDHS Collaboration), Z. Phys. C26, 1 (1983); J.J.Aubert et. al. (EMC collaboration), Nucl. Phys. B259 189 (1985), and *ibid.* B272 158 (1986).

[10] A.C.Benvenuti *et. al.* (BCDMS Collaboration), Phys. Lett. 195B 97 (1987).

[11] G.Curci, W.Furmanski, & R.Petronzio, Nucl. Phys. B175, 27 (1980); W.Furmanski, & R.Petronzio, Phys. Lett. 97B, 437 (1980).

[12] W.Furmanski & R.Petronzio, Z. Phys. C11, 293 (1982).

[13] T.Jaroscewicz, Phys. Lett. 116B, 291 (1982), L.V.Gribov, E.M.Levin, & M.G.Ryskin, Phys. Rep. 100, 1 (1983).

[14] Wu-Ki Tung, "Parton Distribution Functions Incorporating Heavy Quark Mass Effects", in Proceedings of Physics Simulations at High Energies, Ed. V. Barger et. al., Madison, World Scientific, p. 601 (1986).

[15] E. Eichten *et. al.* Rev. Mod. Phys. 56, 579 (1984), and Erratum 58, 1065 (1986).

[16] W.Bardeen, *et. al.* Phys. Rev. D18, 3998 (1978); Floratos et. al. Nucl. Phys. B192, 417 (1981) and reference cited therein.

Table 2: Comparison of 1st- and 2nd-order-evolved Parton Distribution Functions (Input: EHLQ-set 1, Q = 4 GeV)

X	xU(x,Q)_1	xU(x,Q)_2	xG(x,Q)_1	xG(x,Q)_2
		Q = 15 GeV		
1.00E-04	8.26E-01	1.14E+00	3.74E+01	3.35E+01
4.10E-04	6.59E-01	8.47E-01	2.39E+01	2.19E+01
1.67E-03	5.59E-01	6.60E-01	1.46E+01	1.36E+01
6.62E-03	5.25E-01	5.71E-01	8.38E+00	7.93E+00
2.43E-02	5.48E-01	5.62E-01	4.47E+00	4.28E+00
7.29E-02	5.82E-01	5.80E-01	2.19E+00	2.09E+00
1.65E-01	5.47E-01	5.38E-01	9.05E-01	8.63E-01
2.95E-01	4.09E-01	3.99E-01	2.75E-01	2.66E-01
4.50E-01	2.18E-01	2.11E-01	5.35E-02	5.26E-02
6.20E-01	6.95E-02	6.69E-02	4.77E-03	4.97E-03
8.00E-01	7.46E-03	7.13E-03	8.79E-05	9.83E-05
		Q = 100 GeV		
1.00E-04	2.01E+00	2.57E+00	7.98E+01	6.96E+01
4.10E-04	1.34E+00	1.64E+00	4.46E+01	3.95E+01
1.67E-03	9.23E-01	1.07E+00	2.33E+01	2.11E+01
6.62E-03	7.06E-01	7.66E-01	1.12E+01	1.03E+01
2.43E-02	6.22E-01	6.36E-01	4.84E+00	4.50E+00
7.29E-02	5.86E-01	5.79E-01	1.87E+00	1.74E+00
1.65E-01	4.98E-01	4.82E-01	6.15E-01	5.62E-01
2.95E-01	3.35E-01	3.20E-01	1.50E-01	1.38E-01
4.50E-01	1.60E-01	1.50E-01	2.59E-02	2.22E-02
6.20E-01	4.49E-02	4.12E-02	2.19E-03	1.78E-03
8.00E-01	4.08E-03	3.55E-03	4.90E-05	3.28E-05

Table 3: Comparison of DFLM Set-FXNLLA with 2nd-order evolution Calculation (Input: FXNLLA Q = 4 GeV)

X	xU_DFLM	xU(x,Q)_2	xG_DFLM	xG(x,Q)_2
		Q = 15 GeV		
1.00E-04	1.20E+00	1.12E+00	3.10E+01	3.07E+01
4.79E-04	8.70E-01	8.55E-01	1.96E+01	1.95E+01
2.27E-03	6.91E-01	6.80E-01	1.17E+01	1.18E+01
1.03E-02	6.30E-01	6.31E-01	6.57E+00	6.58E+00
4.09E-02	6.50E-01	6.54E-01	3.07E+00	3.08E+00
1.19E-01	6.29E-01	6.30E-01	9.98E-01	1.02E+00
2.49E-01	4.56E-01	4.60E-01	2.51E-01	2.56E-01
4.14E-01	2.25E-01	2.27E-01	5.88E-02	5.88E-02
6.00E-01	6.97E-02	6.97E-02	1.58E-02	1.61E-02
8.00E-01	8.09E-03	7.67E-03	0.00E+00	3.22E-03
		Q = 100 GeV		
1.00E-04	2.49E+00	2.38E+00	6.46E+01	6.42E+01
4.79E-04	1.55E+00	1.51E+00	3.54E+01	3.49E+01
2.27E-03	1.02E+00	1.01E+00	1.76E+01	1.75E+01
1.03E-02	7.60E-01	7.67E-01	7.82E+00	7.81E+00
4.09E-02	6.72E-01	6.79E-01	2.79E+00	2.81E+00
1.19E-01	5.80E-01	5.83E-01	7.16E-01	7.51E-01
2.49E-01	3.75E-01	3.82E-01	1.55E-01	1.61E-01
4.14E-01	1.65E-01	1.68E-01	3.25E-02	3.30E-02
6.00E-01	4.45E-02	4.55E-02	0.00E+00	7.08E-03
8.00E-01	4.17E-03	4.07E-03	0.00E+00	7.70E-04

Table 4: Comparison of MRS Set-EB with 2nd- and 1st-order Evolution Calculations (Input: MRS set at Q = 3.0 GeV)

X	xU_ MRS	xU_2nd	xU_1st	xG_MRS	xG_2nd	xG_1st
			Q = 15 GeV			
1.00E-04	1.28E+00	1.01E+00	7.29E-01	4.67E+01	3.08E+01	3.16E+01
4.10E-04	9.20E-01	7.73E-01	6.01E-01	2.61E+01	2.01E+01	2.05E+01
1.67E-03	6.98E-01	6.22E-01	5.27E-01	1.45E+01	1.26E+01	1.27E+01
6.62E-03	5.82E-01	5.47E-01	5.00E-01	7.98E+00	7.51E+00	7.51E+00
2.43E-02	5.44E-01	5.29E-01	5.11E-01	4.17E+00	4.13E+00	4.12E+00
7.29E-02	5.39E-01	5.34E-01	5.32E-01	1.97E+00	2.01E+00	2.01E+00
1.65E-01	5.13E-01	5.12E-01	5.19E-01	7.75E-01	7.99E-01	8.11E-01
2.95E-01	3.99E-01	4.00E-01	4.10E-01	2.33E-01	2.44E-01	2.51E-01
4.50E-01	2.19E-01	2.20E-01	2.28E-01	4.82E-02	5.09E-02	5.30E-02
6.20E-01	6.88E-02	6.93E-02	7.27E-02	5.30E-03	5.60E-03	5.92E-03
8.00E-01	6.81E-03	6.98E-03	7.45E-03	1.35E-04	1.39E-04	1.49E-04
			Q = 100 GeV			
1.00E-04	2.57E+00	2.04E+00	1.49E+00	9.30E+01	5.99E+01	6.15E+01
4.10E-04	1.57E+00	1.36E+00	1.05E+00	4.52E+01	3.49E+01	3.55E+01
1.67E-03	1.02E+00	9.35E-01	7.77E-01	2.19E+01	1.92E+01	1.94E+01
6.62E-03	7.27E-01	6.99E-01	6.28E-01	1.03E+01	9.75E+00	9.78E+00
2.43E-02	5.97E-01	5.88E-01	5.65E-01	4.44E+00	4.45E+00	4.45E+00
7.29E-02	5.39E-01	5.37E-01	5.38E-01	1.71E+00	1.76E+00	1.77E+00
1.65E-01	4.71E-01	4.72E-01	4.84E-01	5.49E-01	5.74E-01	5.87E-01
2.95E-01	3.34E-01	3.36E-01	3.49E-01	1.37E-01	1.45E-01	1.51E-01
4.50E-01	1.65E-01	1.66E-01	1.75E-01	2.38E-02	2.54E-02	2.68E-02
6.20E-01	4.58E-02	4.61E-02	4.96E-02	2.20E-03	2.31E-03	2.47E-03
8.00E-01	3.80E-03	3.89E-03	4.30E-03	4.03E-05	4.59E-05	4.96E-05

FIGURE CAPTIONS

1. Comparison of first and second order evolved parton distributions. Plotted are x times the probability distributions. Parton species and Q-values are as labelled. Initial distributions at Q = 4. GeV are taken from EHLQ set 1.

2. Comparison of first and second order evolved parton distributions with the corresponding MRS the distributions. Plotted are x times the probability distributions. Parton species and Q-values are as labelled. Initial distributions at Q = 3.0 GeV are the same for all sets.

3. Comparison of DIS scheme and MS-bar scheme parton distributions. Plotted are x times the probability distributions. Parton species and Q-values are as labelled. Initial distributions at Q = 4. GeV are taken from EHLQ set 1.

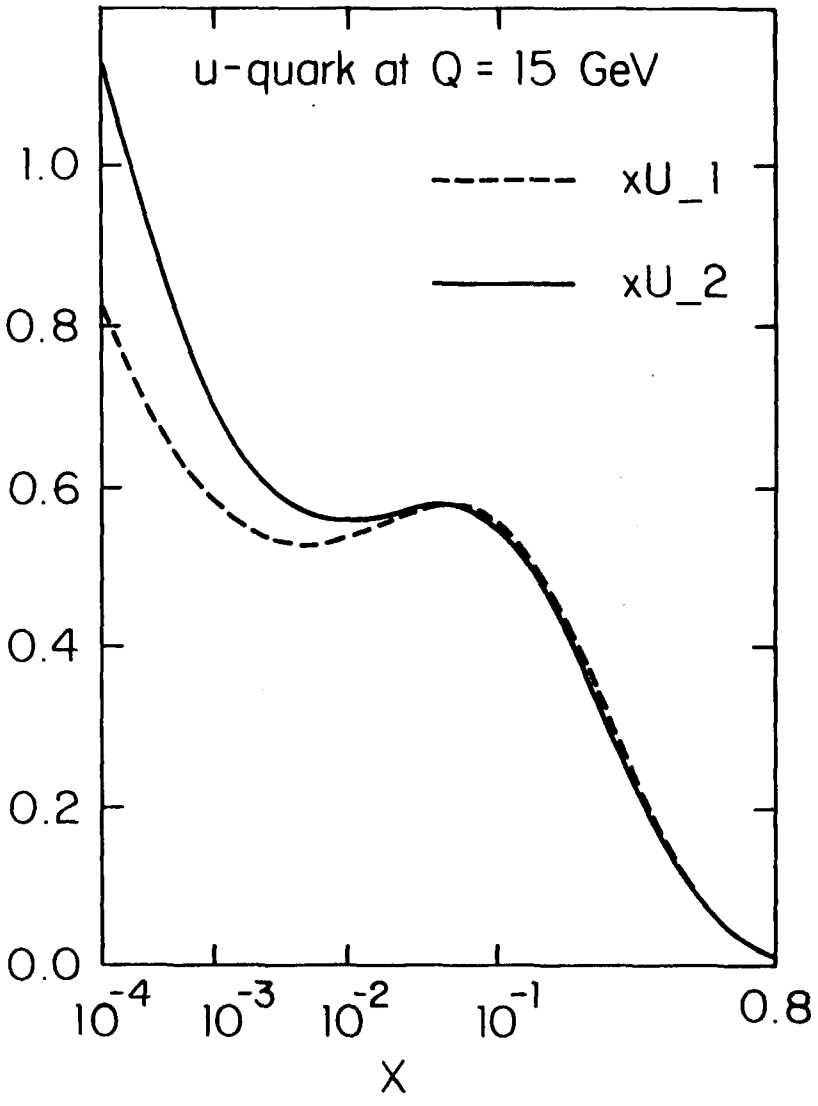
u-quark at Q = 15 GeV
xU_1
xU_2
1.0
0.8
0.6
0.4
0.2
0.0
10^{-4}
10^{-3}
10^{-2}
10^{-1}
0.8
X

(a)

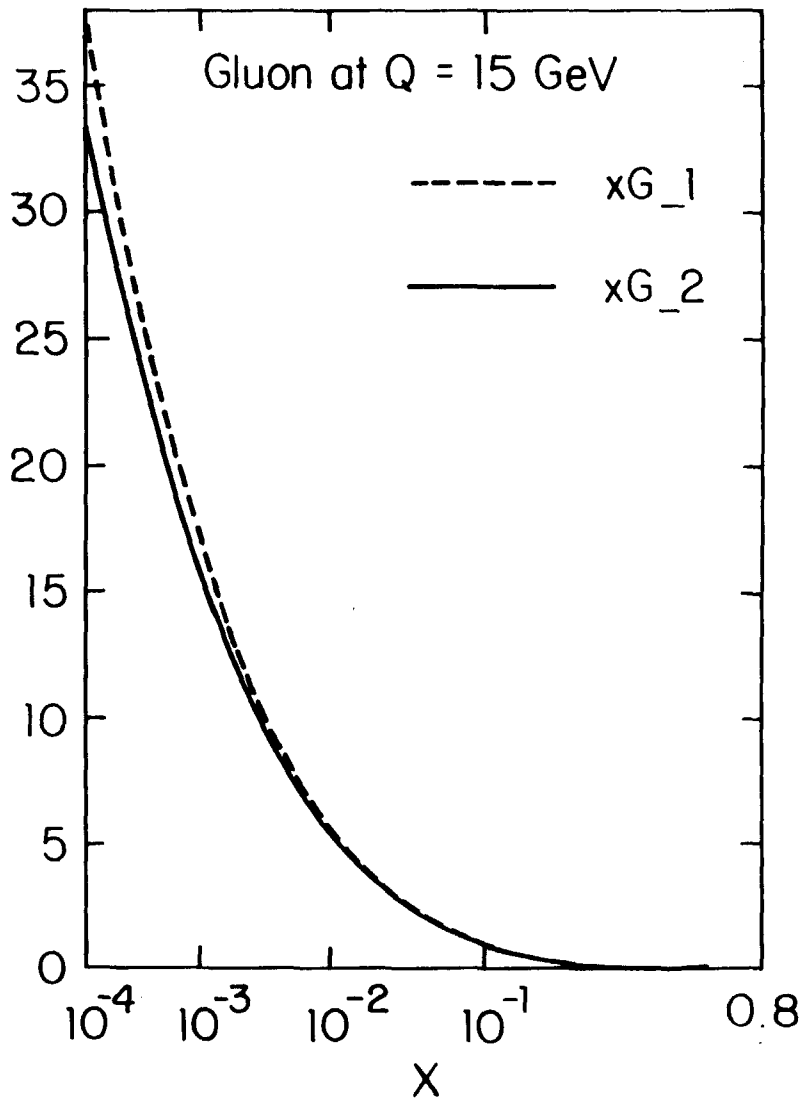
Gluon at Q = 15 GeV
xG_1
xG_2
35
30
25
20
15
10
5
0
10^{-4}
10^{-3}
10^{-2}
10^{-1}
0.8
X

(b)

Fig 1

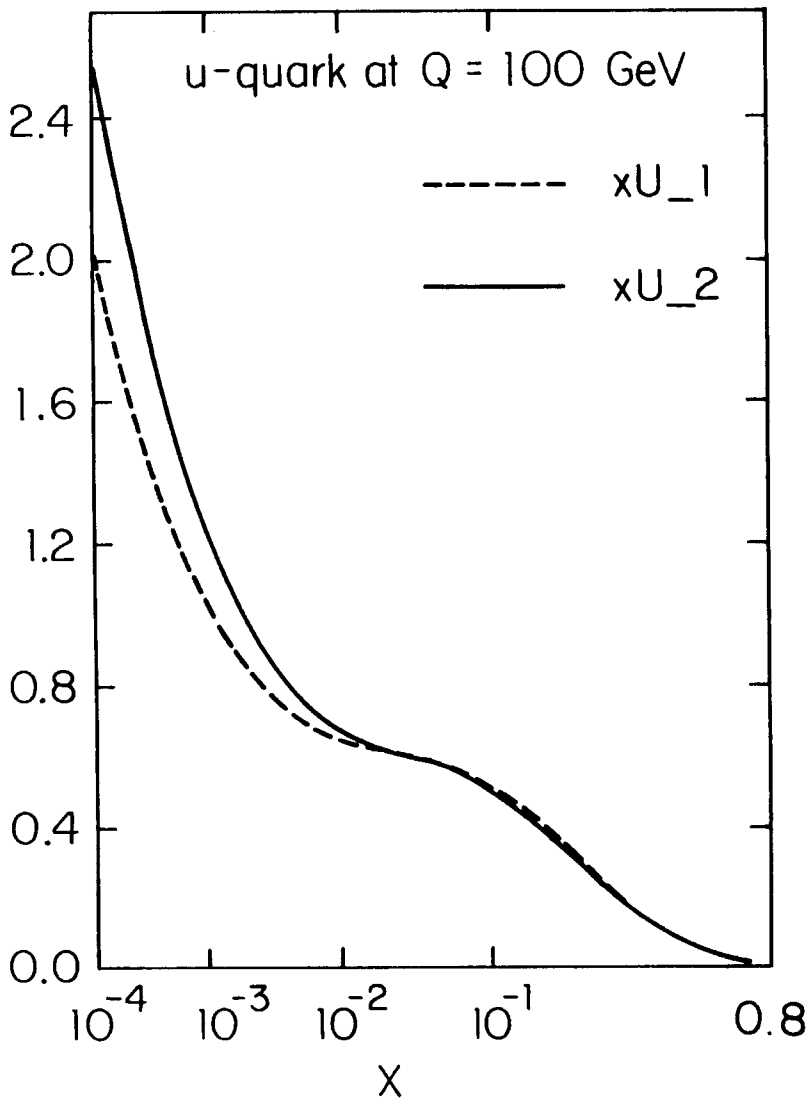
u-quark at Q = 100 GeV
xU_1
xU_2
2.4
2.0
1.6
1.2
0.8
0.4
0.0
10^{-4}
10^{-3}
10^{-2}
10^{-1}
0.8
X

(c)

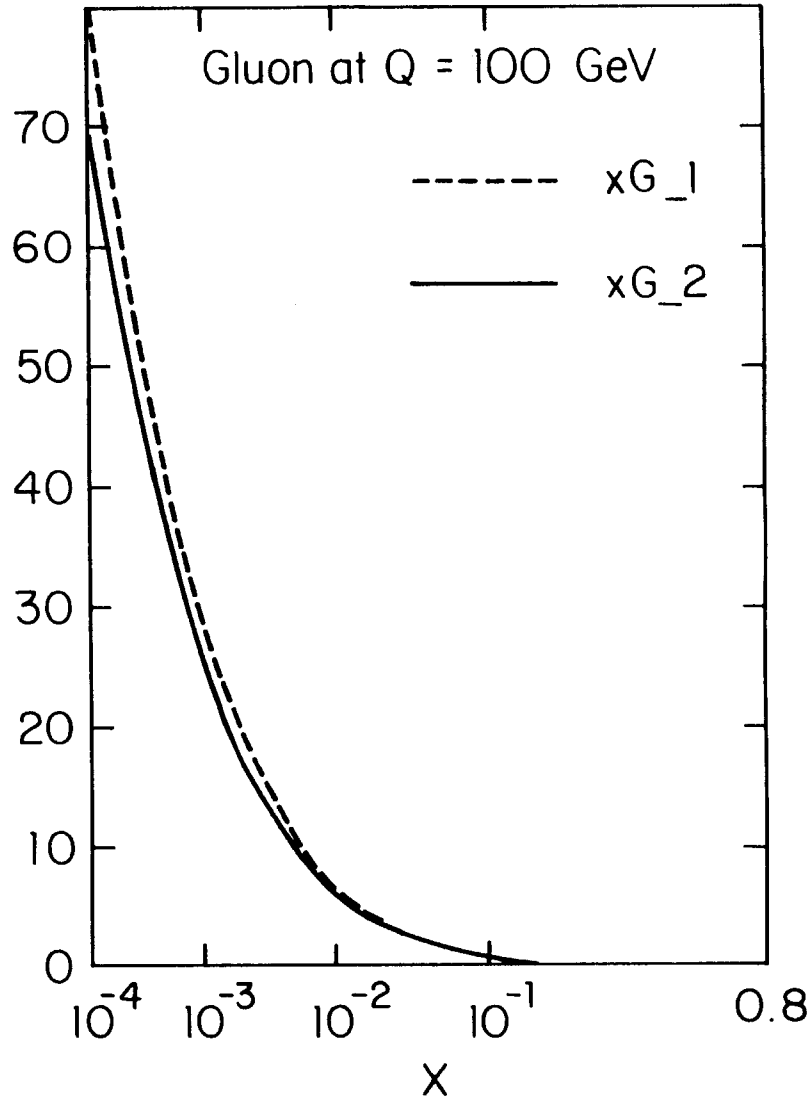
Gluon at Q = 100 GeV
xG_1
xG_2
70
60
50
40
30
20
10
0
10^{-4}
10^{-3}
10^{-2}
10^{-1}
0.8
X

(d)

Fig. 1

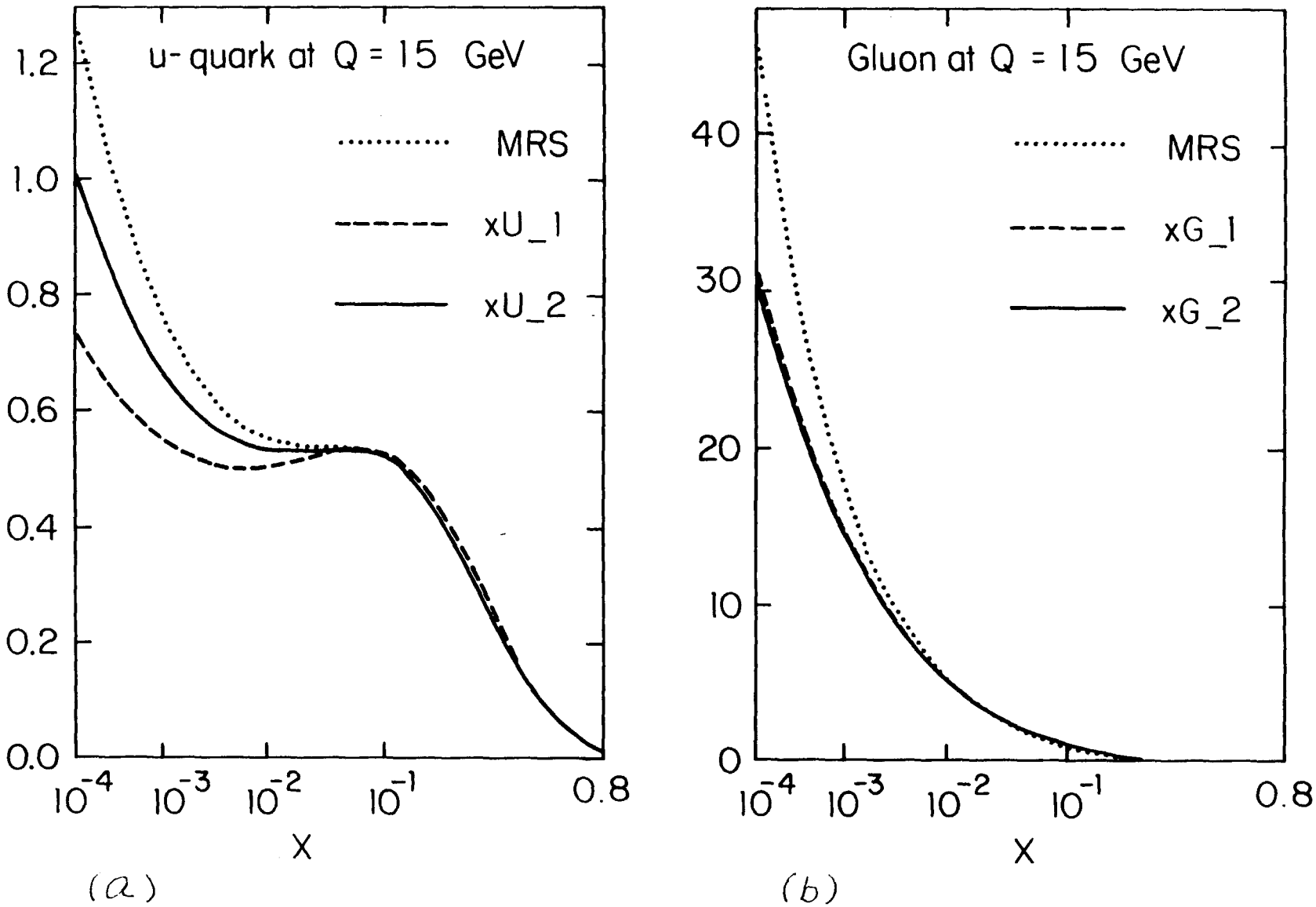
u- quark at Q = 15 GeV
MRS
xU_1
xU_2
1.2
1.0
0.8
0.6
0.4
0.2
0.0
10^{-4}
10^{-3}
10^{-2}
10^{-1}
0.8
X
(a)
Gluon at Q = 15 GeV
MRS
xG_1
xG_2
40
30
20
10
0
10^{-4}
10^{-3}
10^{-2}
10^{-1}
0.8
X
(b)

Fig. 2

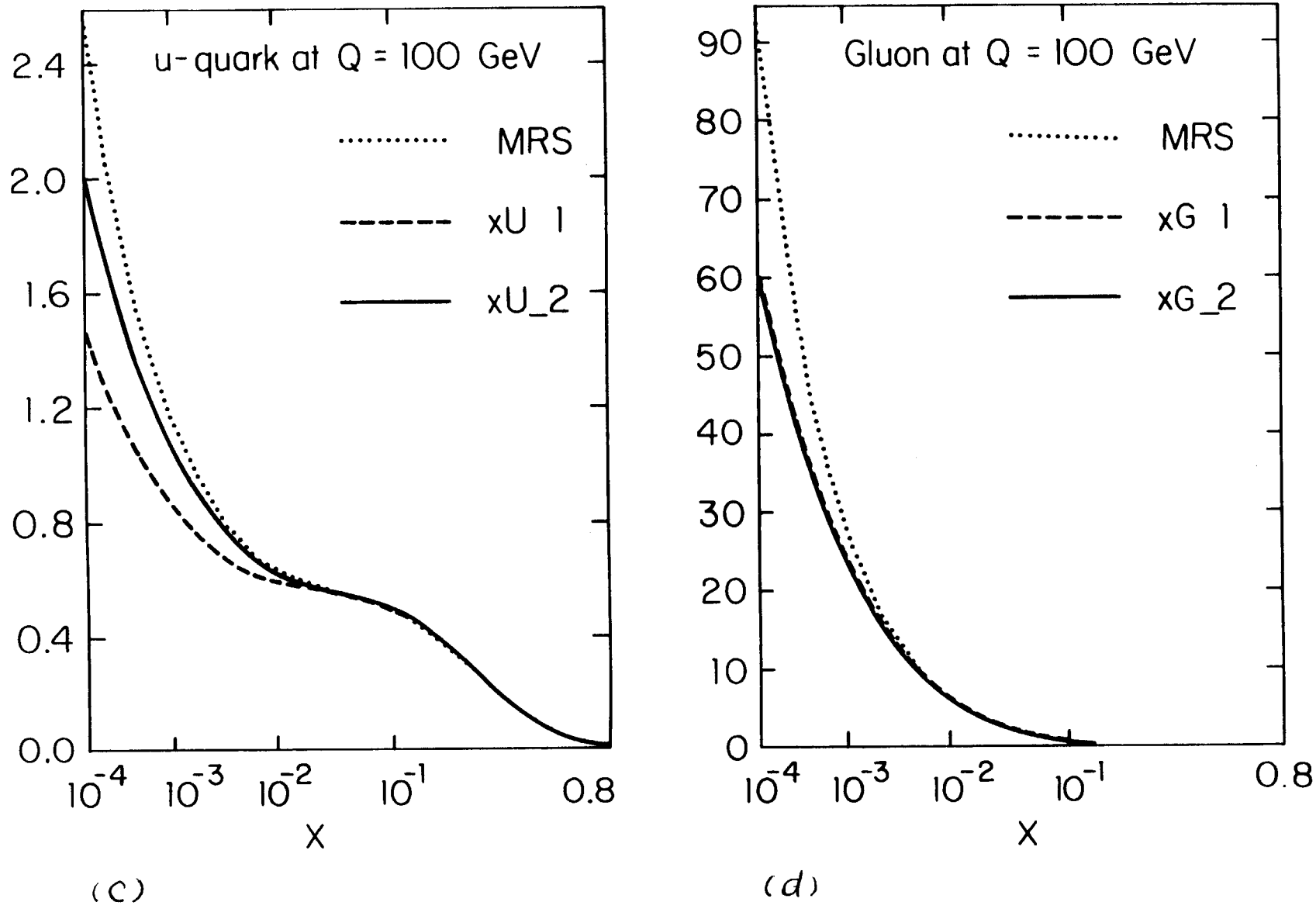
u-quark at Q = 100 GeV
MRS
xU 1
xU_2
2.4
2.0
1.6
1.2
0.8
0.4
0.0
10^{-4}
10^{-3}
10^{-2}
10^{-1}
0.8
X
(c)
Gluon at Q = 100 GeV
MRS
xG 1
xG_2
90
80
70
60
50
40
30
20
10
0
10^{-4}
10^{-3}
10^{-2}
10^{-1}
0.8
X
(d)

Fig. 2

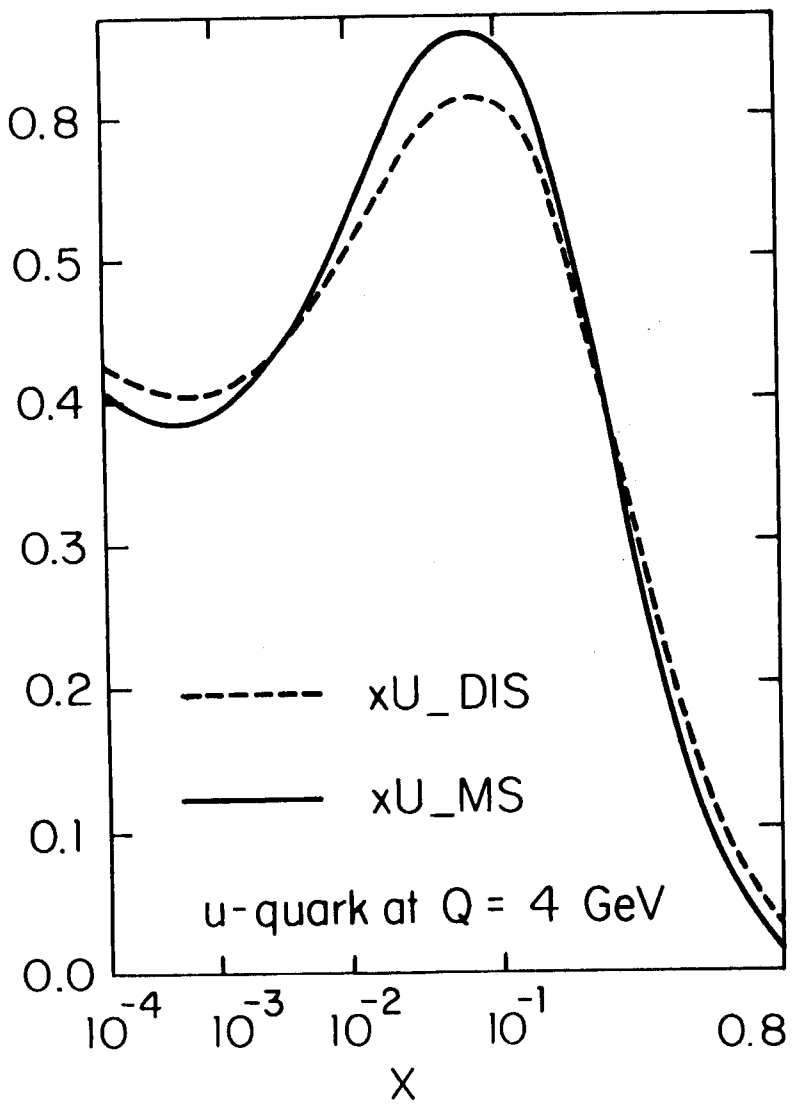
0.8
0.5
0.4
0.3
0.2
0.1
0.0
xU_DIS
xU_MS
u-quark at Q = 4 GeV
10^{-4}
10^{-3}
10^{-2}
10^{-1}
0.8
X

(a)

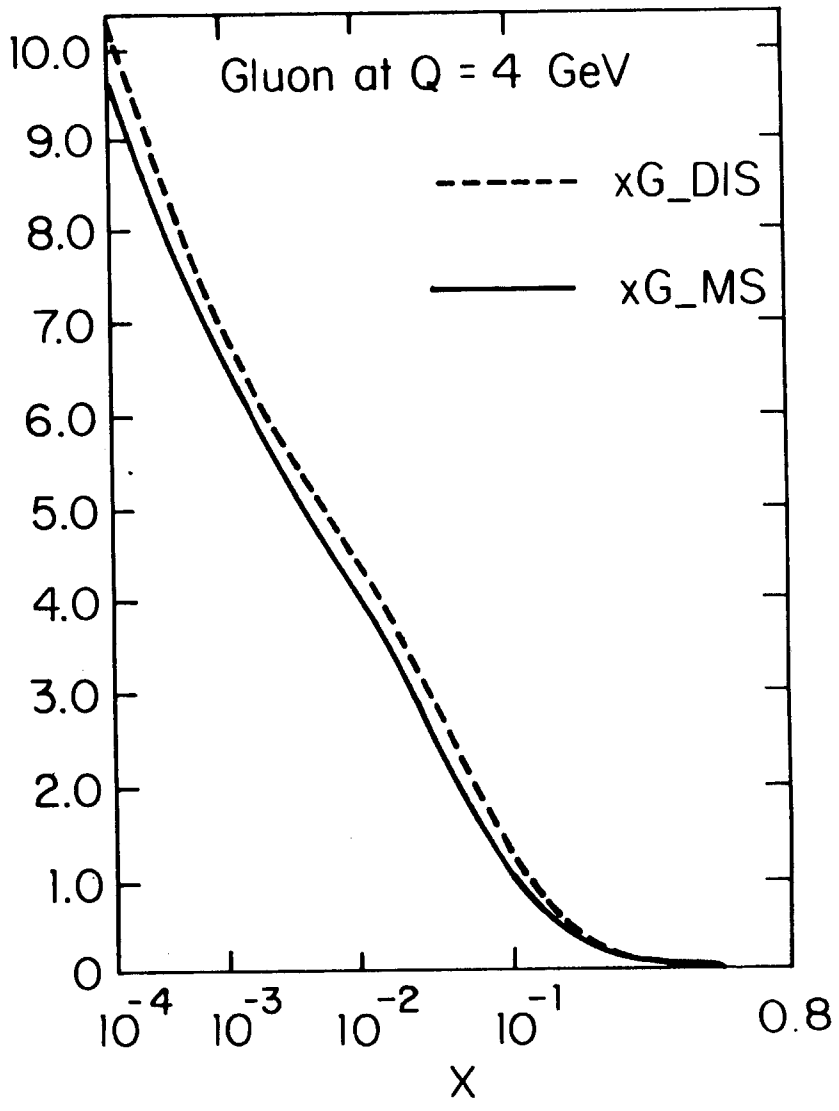
10.0
9.0
8.0
7.0
6.0
5.0
4.0
3.0
2.0
1.0
0
Gluon at Q = 4 GeV
xG_DIS
xG_MS
10^{-4}
10^{-3}
10^{-2}
10^{-1}
0.8
X

(b)

Fig. 3

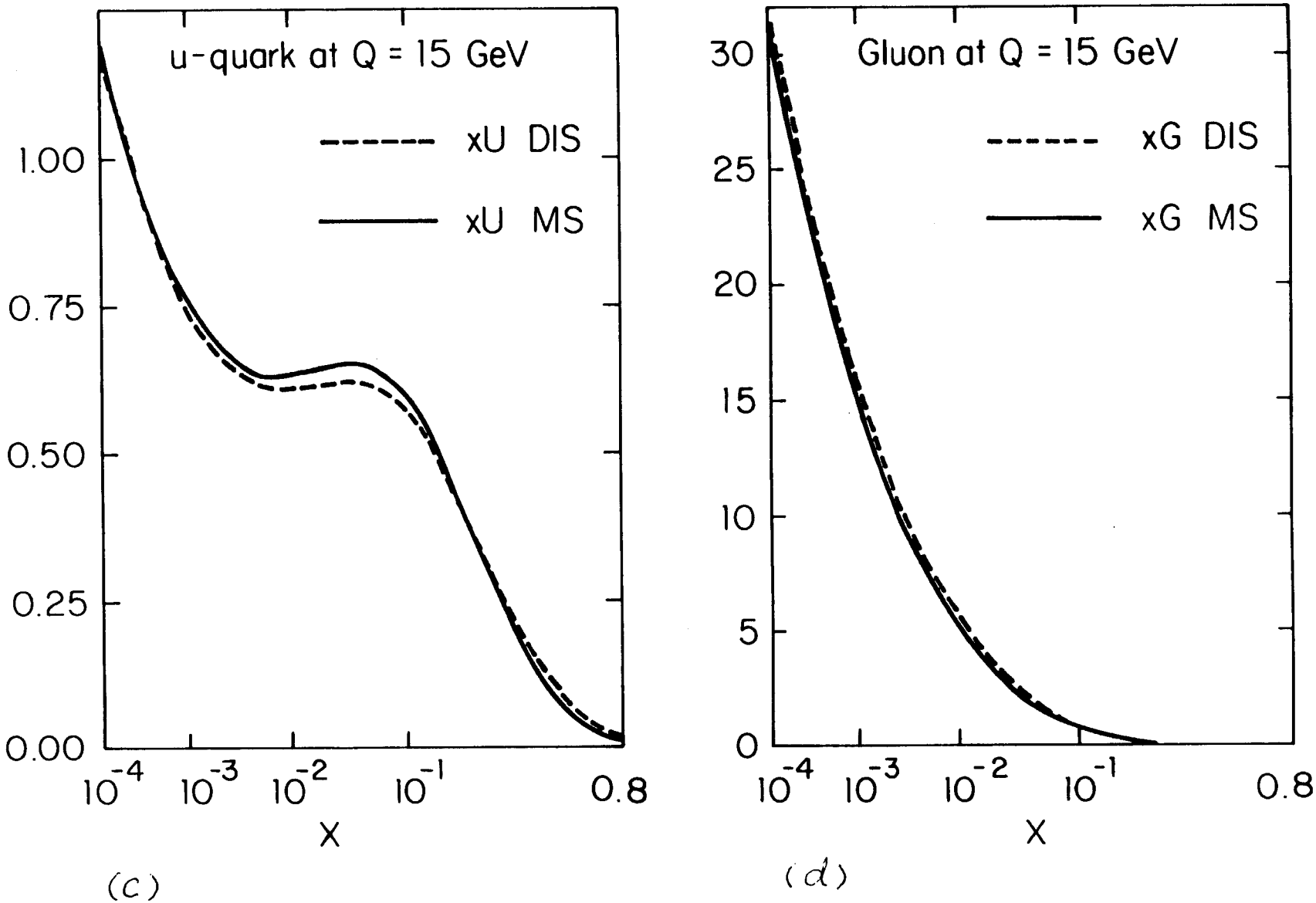
u-quark at Q = 15 GeV
xU DIS
xU MS
1.00
0.75
0.50
0.25
0.00
10^{-4}
10^{-3}
10^{-2}
10^{-1}
0.8
X
(c)
Gluon at Q = 15 GeV
xG DIS
xG MS
30
25
20
15
10
5
0
10^{-4}
10^{-3}
10^{-2}
10^{-1}
0.8
X
(d)

Fig. 3